Ann. Occup. Hyg., 2014, Vol. 58, No. 9, 1186–1199
doi:10.1093/annhyg/meu064
Advance Access publication 3 September 2014

BOHS The Chartered Society for Worker Health Protection

Simulated Effects of Head Movement on Contact Pressures between Headforms and N95 Filtering Facepiece Respirators Part 2: Simulation

Zhipeng Lei[1], Xuewu Ji[2], Ning Li[1], James Yang[1]*, Ziqing Zhuang[3] and Dana Rottach[3]

1.Human-Centric Design Research Laboratory Department of Mechanical Engineering Texas Tech University, Lubbock, TX 79409, USA
2.State Key Lab of Automotive Safety and Energy Tsinghua University, Beijing 100084, China
3.National Institute for Occupational Safety and Health, Pittsburgh, PA 15236, USA
*Author to whom correspondence should be addressed. Tel: +1-806-834-6746; fax: +1-806-742-3540; e-mail: james.yang@ttu.edu
Submitted 14 March 2014; revised 16 July 2014; revised version accepted 16 July 2014.

ABSTRACT

Finite element (FE) filtering facepiece respirators (FFRs) were developed and mated to the new headforms with a cervical spine model. The FFRs from three manufacturers included three sizing systems: (i) a single one-size-fits all, (ii) an FFR with two sizes (S/M and M/L), and (iii) an FFR with three sizes (S, L/M, XL). Finite element method (FEM) simulations of 16 headform and respirator combinations (5 headforms and 6 respirators) were used to examine maximum contact pressure changes for five cases: static head, flexion, extension, left rotation, and right rotation. For each of the 16 headform and respirator combinations, maximum contact pressures of the static headform and motile headforms were compared using *t*-tests. Significant differences on the maximum contact pressures were found in the extension, left rotation and right rotation at the nose ($P < 0.005$), the left rotation at the top of right cheek ($P = 0.03$), and the extension at the bottom of left/right cheek ($P = 0.01$). When separately considering each headform and each FFR manufacturer, the effects of the four head movement cases on the nose maximum contact pressure changes were observed in the simulations with all five headforms and all FFR manufacturers. The effects of the left and right rotations on the chin maximum contact pressure changes were observed in the simulations with the small headform. It was also found that the use of a nose clip could reduce the impact of the head left/right rotations on nose maximum contact pressure changes. In addition, head movements changed pressure contours of the key nose area. Caused by the head movements, the maximum contact pressure changes may affect seal quality, and the increase of the maximum contact pressures could reduce the facial comfort level.

KEYWORDS: finite element simulation; head movement; respirator contact pressure

INTRODUCTION

In respirator fit testing, test exercises are considered as an important component for evaluating respirator protection for the wearer. The exercises, including normal breathing without talking, deep breathing, moving the head side to side, moving the head up and

down, and talking, are commonly required (OSHA, 1999). The contact between a respirator and a static headform has been simulated by Lei *et al.* (2012), and the normal breathing and the deep breathing exercises with the respirator usage has been simulated by Lei *et al.* (2013). This study describes simulations of two additional exercises: turning the head side to side and moving the head up and down with the respirator donned.

In the real world, respirator users move their head during most tasks. In the respirator fit test, exercises involving turning the head side to side and moving the head up and down were chosen to mimic common head movements in the workplace. The head movement exercises increased faceseal leakage in respirators. Crutchfield *et al.* (1999) found that performing the fit test exercises, including these gross head movements, affects the elastomeric respirator seal on human subjects. Lee *et al.* (2005) reported that the fit test exercises impacted the N95 filtering facepiece respirator (FFR) fit on a human subject. Grinshpun *et al.* (2009) found that head movement exercises lower the measured fit levels of N95 FFR, while did not affect human inspiratory flow rates.

The tendency of the respirator to change contact properties across the face during gross head motions has not previously been studied. In a previous study, a finite element (FE) FFR was applied to a headform without head movement and contact was simulated (Lei *et al.*, 2012). Headforms were from the National Institute for Occupational Safety and Health (NIOSH), including five sizes of headforms (small, short/wide, medium, long/narrow, and large) (Zhuang *et al.*, 2010). FE NIOSH headform models, having multiple layers for the skin, muscle, fatty tissue, and bone were built, and FE FFR models, with a facepiece, two straps, and a deformable nose clip were developed. However, head movements were not modeled in the previous study. Air flows and heat transfer in the FFR cavity with the normal breathing and the deep breathing were later simulated using computational fluid dynamics (CFD) (Lei *et al.*, 2013).

The ultimate goal of this study is to develop computer-based methods to simulate all of the exercises performed in the respirator fit test. The new headforms described previously are used here to investigate the effect of headform movement on maximum contact pressures between FFR and headforms. In addition, a potential connection between head movement and respirator leaks and comfort levels is investigated based on changes in the maximum contact pressure.

METHODS

In this article, we use the integrated head and spine model presented in the companion paper (Lei *et al.*, 2014) along with FE FFR models from an earlier phase of this research (Lei *et al.*, 2010a, 2010b). The spine model had cervical vertebrae C0–C7. The initial static contact between the headform model and the FFR model was simulated. Forces (moments) were then applied to the model to simulate gross head movements.

FE FFR models

Six FFR models generated in our previous study, including a one-size FFR (3M 8210), two-size small/medium and medium/large FFRs (MOLDEX 2200 and MOLDEX 2201), and three-size large, medium and small FFRs (SPERIAN XL, SPERIAN L/M and SPERIAN S), were used (Lei *et al.*, 2010a, 2010b). The development of each FE FFR model was based on measurements of sample FFRs. For example, the FE 3M 8210 model had a facepiece (with an inner layer and an outer layer), a nasal clip and two straps. The filtering facepiece of the FFR sample was scanned by a Cyberware rapid 3D digitizer (Monterey, CA, USA). The scanned surface was processed to generate an FE shell of the facepiece as a set of triangle elements. A duplicate of the first shell was created and offset to form the outer surface. By offsetting the shell, two layers of pentahedral solid elements were obtained as two layers of the FE facepiece model. FE models of the two straps were separately built as two rectangular bars. Lengths, widths and heights of the straps were determined from the 3M 8210 sample. The FE model of the nasal clip was conformingly fixed on the surface of the facepiece. The shape and position of the nasal clip were obtained from the nasal clip in the 3M 8210 FFR sample. Other FE FFR models were created in a similar way.

Table 1 lists the components of the six FFR models, as well as dimensions, densities and mechanical properties. The FFR components were set as elastic materials with Young's modulus (E) and Poisson's ratio (v). The FFR facepieces, which were nonwoven material, were assigned a Poisson's ratio of 0.40 (Sun *et al.*,

Table 1. Properties of FFR models

	Dimension	Density (10^3 kg m^{-3})	*E* (MPa)
3M 8210			
Upper strap	310 × 6.5 × 0.6 mm	1.06	10.2
Lower strap	250 × 6.5 × 0.6 mm	1.06	10.2
Inner facepiece	18 200 mm^2, thick 1 mm	1.39	9.5
Outer facepiece	18 200 mm^2, thick 2 mm	1.39	4.5
Nasal clip	90 × 5 ×1 mm	1.1	
Moldex 2200			
Upper strap	287 × 6.25 × 0.41 mm	1.06	6.25
Lower Strap	240 × 6.25 × 0.41 mm	1.06	6.25
Inner facepiece	2463 mm^2, thick 2 mm	0.5	0.37
Outer facepiece	21 288 mm^2, thick 1 mm	1.39	2.1
Moldex 2201			
Upper strap	287 × 6.25 × 0.41 mm	1.06	6.25
Lower Strap	240 × 6.25 × 0.41 mm	1.06	6.25
Inner facepiece	1602 mm^2, thick 2 mm	0.5	0.37
Outer facepiece	20 210 mm^2, thick 1 mm	1.39	2.1
Sperian XL			
Upper strap	235 × 5 ×0.4 mm	1.06	6.25
Lower Strap	200 × 5 ×0.4 mm	1.06	6.25
Inner facepiece	4417 mm^2, thick 2 mm	0.3	0.1
Outer facepiece	21 286 mm^2, thick 1 mm	1.39	3
Nasal clip	88 × 8 ×1 mm	1.1	
Sperian M/L			
Upper strap	235 × 5 ×0.4 mm	1.06	6.25
Lower Strap	200 × 5 ×0.4 mm	1.06	6.25
Inner facepiece	4373 mm^2, thick 2 mm	0.3	0.1
Outer facepiece	20 730 mm^2, thick 1 mm	1.39	3
Nasal clip	88 × 8 ×1 mm	1.1	
Sperian S			
Upper strap	225 × 5 ×0.4 mm	1.06	6.25
Lower Strap	195 × 5 ×0.4 mm	1.06	6.25
Inner facepiece	1999 mm^2, thick 2 mm	0.3	0.1
Outer facepiece	18 120 mm^2, thick 1 mm	1.39	3
Nasal clip	88 × 8 ×1 mm	1.1	

2005), and the straps, which were modeled as rubber, were assigned a Poisson's ratio of 0.48. The Young's modulus values of straps were measured in material testing laboratory at Texas Tech University, and the Young's modules values of the FFR facepieces were obtained from Schaff and Ogale (1991). The nasal clip material was modeled as malleable aluminum in the beginning of a contact simulation, changing to a rigid material in the middle of the contact simulation, as described below. The Moldex 2200 and 2201 models did not have a nasal clip.

Contact simulations of headform/FFR with head movements

The NIOSH headforms represent five head sizes in the NIOSH principal component analysis (PCA) panel. Zhuang *et al.* (2008) provided recommended combinations of headform sizes and respirator sizes. The current study considered the recommended combinations of headform/FFR and excluded other combinations. Tested headform/FFR combinations are marked with an 'X' in Table 2.

A method to simulate the contact between an FE FFR and a headform without head movement was developed in a previous study (Lei *et al.*, 2012). The contact simulations were conducted using the LS-DYNA finite element analysis package (Livermore Software Technology Corporation, Livermore, CA, USA). In this study, the method was extended to study the fixed headform and four motile cases: flexion, extension, left rotation, and right rotation. Step 1 involved simulating the pull of the straps around the back of the headform. The facepiece was held ~10 mm away from the headform frontal surface. The nodes on the headform were all fixed. The ends of the straps moved from the posterior side of the headform to the facepiece. The straps contacted the back of the headform, deforming the straps and producing internal stresses. Step 2 involved simulating the attachment of the straps to the facepiece and release of the facepiece. The tension of the straps pulled the facepiece toward the headform and the facepiece began to contact the face of the headform. During the contact phase, the facepiece and headform both underwent deformation. At the end of this step, the motion and the deformation of the facepiece was stable and did not change with further simulation time.

Step 3 involved manipulating the nasal clip for molding the shape of the nasal bridge. A simulated 2N force was applied to each side of the nasal clip tip for 0.1 s to deform the nasal clip to the contours of the face. The material property of the simulated nasal clip was then switched from elastic to rigid. After the forces on the tips of the nose clip were removed, the nose clip was not allowed to revert to its original shape but retained the shape of the nasal bridge. No attempt was made to fit the FFR to the face by simulating a seal check at the initial seating.

Step 4 involved rotating the headform to the desired head orientation. A global coordinate system was defined where the origin was located at the point of the nasal tip, the *z*-axis was normal to the headform frontal face, the *x*-axis was along the lateral direction of the headform towards the headform frontal face's left, and the y-axis was defined by the right hand rule. Seven local coordinate systems of C0–C1 to C6–C7 were defined for the relative movements of C0–C1 to C6–C7. The axes of the

Table 2. The tested headform/FFR combinations, marked with 'X'

FFR	Headform				
	Small	**Short/wide**	**Medium**	**Long/narrow**	**Large**
3M 8210	X	X	X	X	X
Moldex 2201	X	X	X		
Moldex 2200			X	X	X
Sperian S	X	X			
Sperian M/L			X		
Sperian XL				X	X

local coordinate systems were parallel to the *X*-, *Y*- and *Z*-axes of the global coordinate system. The full descriptions of the coordinate systems were in Lei *et al.*, 2014. For the fixed head case, no external load was applied to the headform. In the head movement cases, pure moment loads were applied to the back of the head along the axes of C6–C7 local coordinate system for flexion (M_x = 2.0 Nm), extension (M_x = −2.0 Nm), left rotation (M_y = 1.00 Nm), and right rotation (M_y = −1.00 Nm).

At the final state of each simulation the head was stationary. Fig. 1 shows the final states of five simulations of the medium headform/ 3M 8210 combination. The relative movements of C0–C1 to C6–C7 were defined as the rotation angles of C0–C1 to C6–C7 around their corresponding local coordinate axes. A final head positions was calculated as the summation of the rotation angles of C0–C1 to C6–C7 at the final simulation state. Figure 2 shows pressure distributions in the final states of the five simulations of the medium headform/3M 8210 combination.

Table 3 summarizes the test conditions for contact simulations of the 16 headform/FFR combinations. For each combination, there were five simulations for five cases including the fixed (static) head, flexion, extension, left rotation, and right rotation. Thus, there were (16×5) 80 simulations in total, and among them, (16×4) 64 simulations included head movements. The final head position was determined as the summation of C0–C7 joint rotation angles at the final states of the simulations. Pressure distributions on the headform surface were also determined at the final states of the simulations.

To quantitatively evaluate effects of the head movements on the pressure distributions, six key areas were defined, including (i) the nose, (ii) the top of the left cheek, (iii) the top of the right cheek, (iv) the bottom of the left cheek, (v) the bottom of the right cheek, and (vi) the chin, as shown in Fig. 3. The reason to choose these six key areas is that all had high contact pressures and similar contact pressure distribution patterns. In each key area, maximum contact

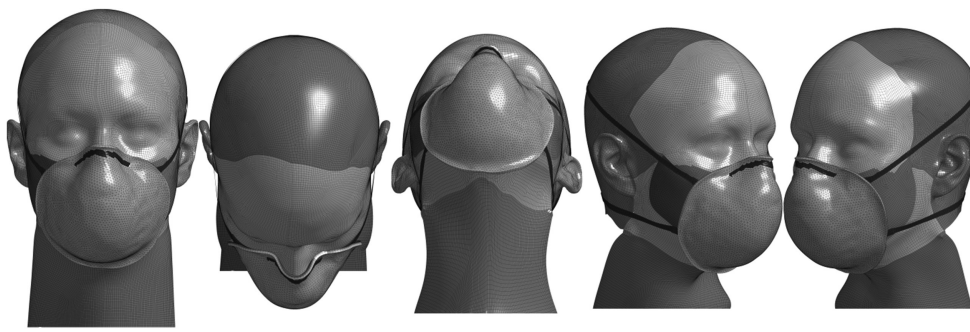

1 Final states of five simulations of the medium headform/3M 8210 combination: (a) Fixed head; (b) flexion; (c) extension; (d) left rotation; (e) right rotation.

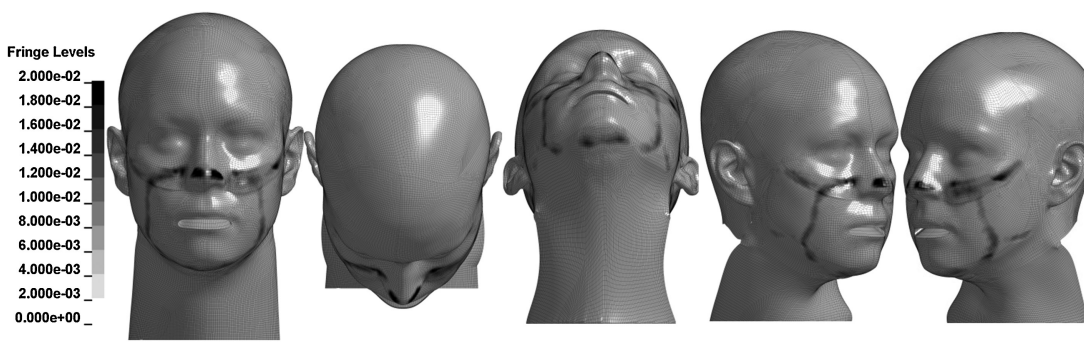

2 Pressure distributions in the final states of five simulations of the medium headform/3M 8210 combination: (a) Fixed head; (b) flexion; (c) extension; (d) left rotation; (e) right rotation.

Table 3. A summary of test conditions for contact simulations of headform/FFR combinations under five head movements

Name	Number
Sizes of headforms	5
Sizing systems of FFRs	3
Properly fitted headform/FFR combinations	16
Total head situations	5
Head movement cases	4
Total contact simulations	80
Contact simulations with head movements	64
Key areas for contact pressures	6

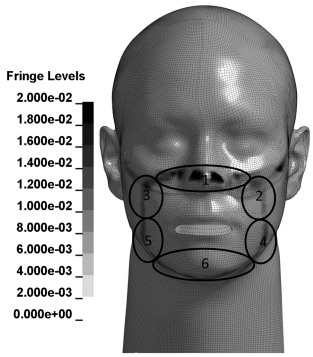

3 Six key areas: (1) the nose, (2) the top of the left cheek, (3) the top of the right cheek, (4) the bottom of the left cheek, (5) the bottom of the left cheek, and (6) the chin.

pressure appeared at the center of the key area, and small contact pressures (below 0.004 MPa) appeared at the junction between two key areas. Zero contact pressures are likely potential facial leak locations. The pressure distribution pattern can be explained by the anatomy of human face and the FFR structure. The key areas of the nose and the chin covered the nasal bone and the mandible with thin soft tissue about 2 and 4 mm thicknesses, respectively, while the soft tissue thickness of the cheek key area was about 15 mm. It is reasonable to expect that the bony prominences from the nasal bone and the mandible may lead to high contact pressures on the key area centers of the nose and the chin. The four ends of the FFR straps connected to the FFR facepiece at locations touching the key area centers of the left/right cheek tops and the left/right cheek bottoms. Hence, the strap forces were directly exerted on these four key area centers, generating higher contact pressures than exhibited nearby.

A maximum contact pressure value at each key area was determined. There were $(16\times5\times6)$ 480 maximum contact pressures in total. The maximum contact pressure was chosen for two reasons. First, it is readily accessible from the simulation results. It may be argued that leaks are to be found in areas with low contact rather than high, but as there are portions for each face mask that do not contact the skin and therefore these portions must have no contact pressure, using a least contact pressure measure is impractical for the purposes of this study. Note that it is impossible to consider the average contact pressure for each defined key area because the area of contact for each key area changes with head movements.

Secondly, and more importantly, it is expected that the maximum contact pressure will be strongly correlated with faceseal leakage and comfort. A low value of the maximum contact pressure (close to zero) indicates that the respirator sealing at the key area is inadequate and leaks are likely to appear. If the contact pressures were uniformly distributed no leaks would be likely with usual strap tension. However, in reality the contact pressures are not evenly distributed. A high value of the maximum contact pressure (above 0.04 MPa) indicates that the contact pressure distribution is not even. When regions have locally high contact pressures, the contact pressures in the surrounding areas are likely to decrease in compensation, causing face seal leakage. For example, a high pressure spot between the nose and the nasal-clip supported region of the FFR may cause a low pressure spot nearby, where the FFR does not conform to shape of the face adequately. In addition, when the contact pressure is higher the facial comfort level is expected to be lower.

RESULTS

For contact simulations with the fixed head, the final head positions remained at 0°. Means and standard deviations of the final head positions for the four head movements were calculated at the end of the contact simulations with head movement. For example, there were 16 contact

simulations in which the head moved down (flexion), and thus 16 simulated final head positions for flexion. The mean and standard deviation of the 16 final head positions for flexion were obtained as 67.85°(1.11°). Similarly, the means and standard deviations were obtained as −63.13°(0.64°) for extension, 48.49°(1.16°) for left rotation, and −48.39°(1.20°) for right rotation. The standard deviations were relatively small compared to the mean values (below 3% of the mean values).

For each headform/FFR combination, maximum contact pressures at the six key contact areas under five head movements were determined. Fig. 4a presents maximum contact pressures at the six key areas for the medium headform/3M 8210 combination

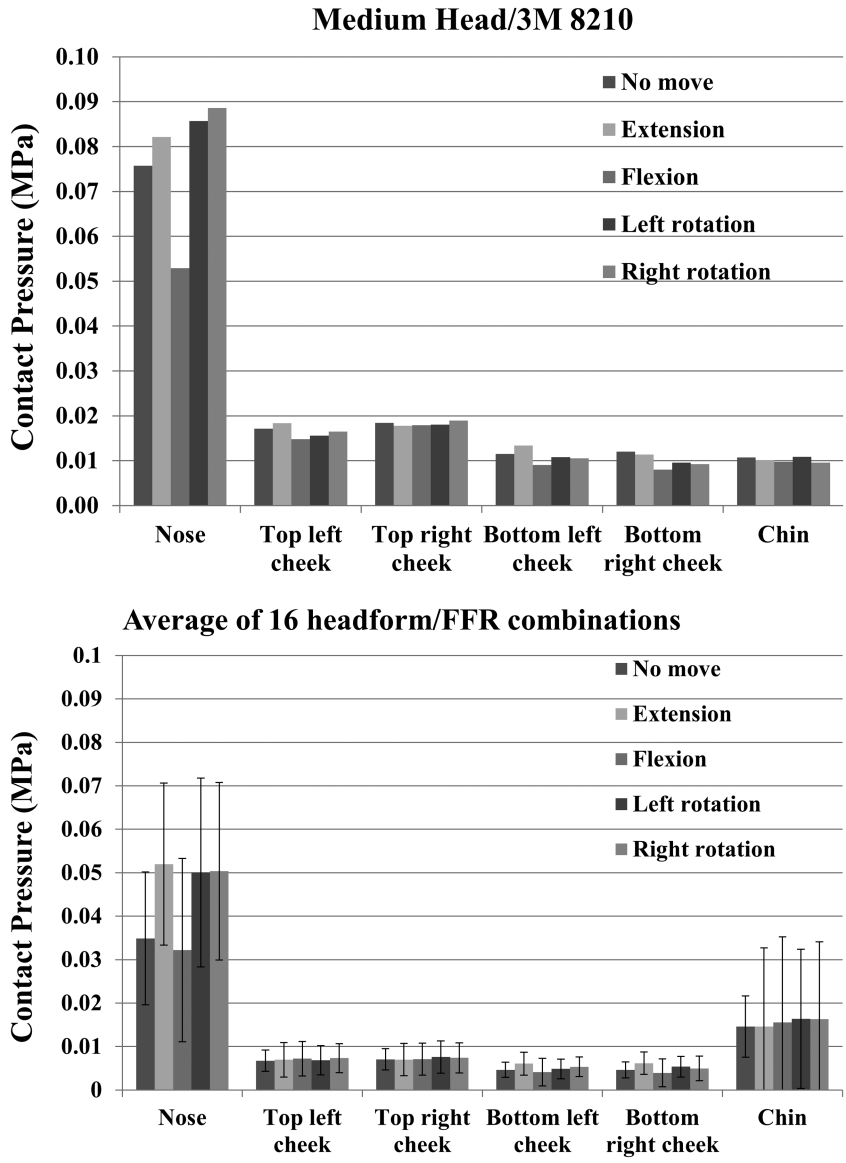

4 Maximum contact pressures: (a) Medium headform/3M 8210 combination; (b) means and standard deviations for the 16 headform/FFR combinations, at six key areas under five head movement cases.

Table 4. Results of the t-test that tested the difference in the maximum pressure values of a key area between a simulation with fixed head and a simulation with one of four head movement cases (two-tail, paired two samples for means)

Head movements	*P* value					
	Nose	Top of left cheek	Top of right cheek	Bottom of left cheek	Bottom of right cheek	Chin
Flexion	0.55	0.13	0.84	0.13	0.13	0.26
Extension	<0.005	0.62	0.89	0.01	0.01	0.98
Left rotation	<0.005	0.83	0.03	0.69	0.09	0.21
Right rotation	<0.005	0.11	0.37	0.12	0.37	0.22

under five head movements. Similarly, maximum contact pressures for other headform/FFR combinations were recorded and are included in the supplemental documents. For a head movement and a key area, the maximum contact pressures were determined in 16 headform/FFR combinations and their mean and standard deviation were calculated. Fig. 4b shows the means and standard deviations of maximum contact pressures at six key areas for the 16 headform/FFR combinations under five head movements.

The maximum contact pressures under the fixed head case were set as a baseline, and compared with maximum contact pressures under one of the head movement cases using a two-tailed *t*-test of paired two samples for means. For example, the nose maximum contact pressures from 16 simulations with fixed head case were compared with those with head extension ($P < 0.005$). Table 4 provides results of *t*-tests for each key area between the fixed head case and any one of the four head movement cases (two-tail, paired two samples for means). *P*-values for the extension/nose, left rotation/nose and right rotation/nose were below 0.005, and for the left rotation/top of right cheek, extension/bottom of left cheek, and extension/bottom of right check were below 0.05.

The 16 headform/FFR combinations were grouped according to headform size. For example, for each key contact area and each head movement case, the large headform had three headform/FFR combinations and mean and standard deviation were obtained from the three maximum contact pressures. Fig. 5 shows the mean and standard deviation of maximum contact pressures at six key areas for each headform under five head movement cases. Similarly, the 16 headform/FFR combinations were grouped by three FFR manufacturers. Fig. 6 presents the mean and standard deviation of maximum contact pressures at six key areas for each FFR manufacturer under five head movement cases.

DISCUSSIONS

The head movement was driven by an external moment in the simulation examples. Four separate external moments generated the four head movement cases. The variation in the headform final positions for each head movement case was due to the different size headforms. The headforms had different dimensions and different tissue thicknesses, which affected the overall effective stiffness of the headform models. Different FFR models in the simulations also slightly affected the headform final position. However, the variations were much smaller than the mean values (the standard deviation below 3% of the mean). The results showed that with the same external moment applied all final head positions of the 16 headform/FFR combinations were similar. The headform models provided a feasible way to achieve head movements in headform/FFR contact simulations through applying external moments.

The overall averages of maximum contact pressure changes for the 16 headform/FFR combinations were used to investigate the effects of head movements. The extension and left/right rotations largely increased the average maximum contact pressure at the nose by 0.018 and 0.014 MPa compared with the fixed head case. Using *t*-tests, it was found that the extension, left rotation and right rotation significantly changed the maximum contact pressures at

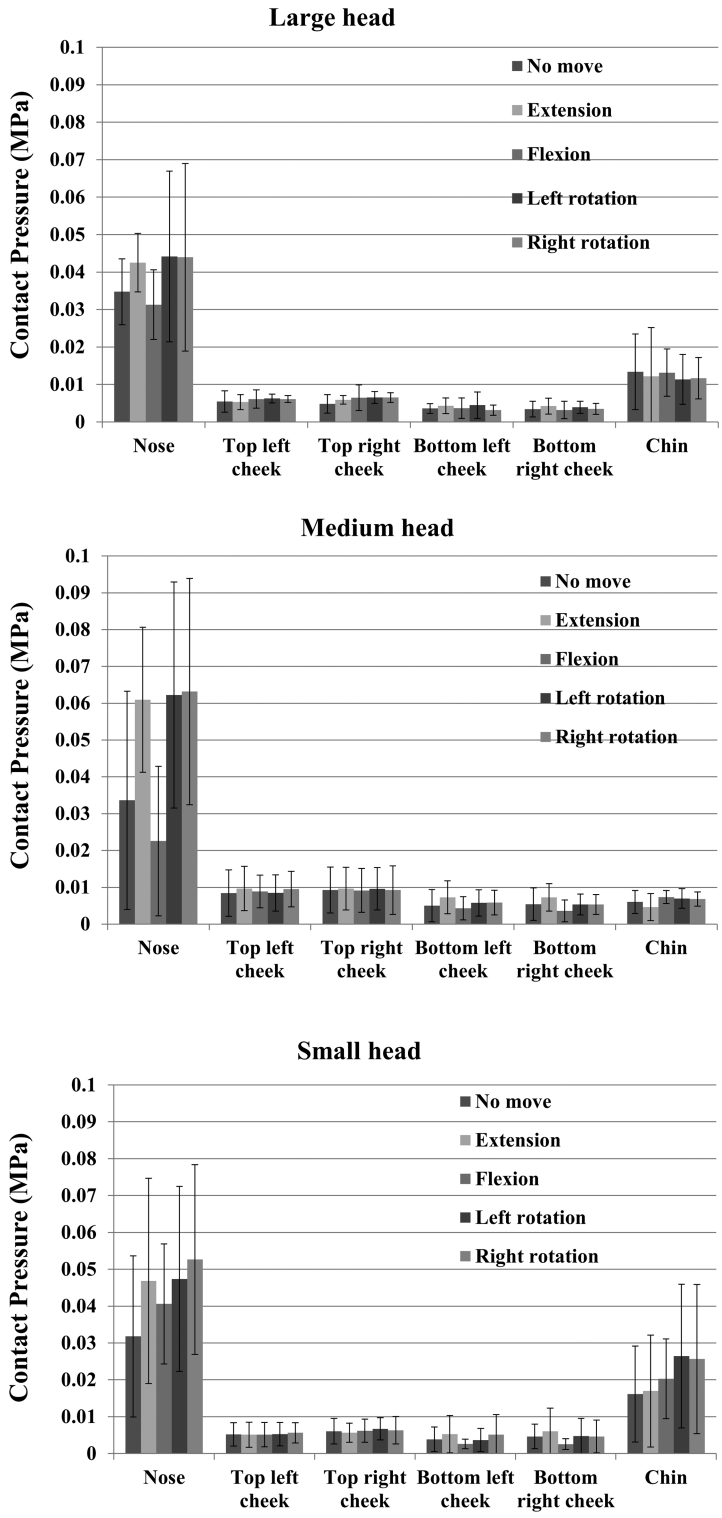

5 Means and standard deviations of maximum contact pressures at six key areas for contact simulations under five head movement cases: (a) Large head; (b) medium head; (c) small head; (d) short/wide head; and (e) long/narrow head.

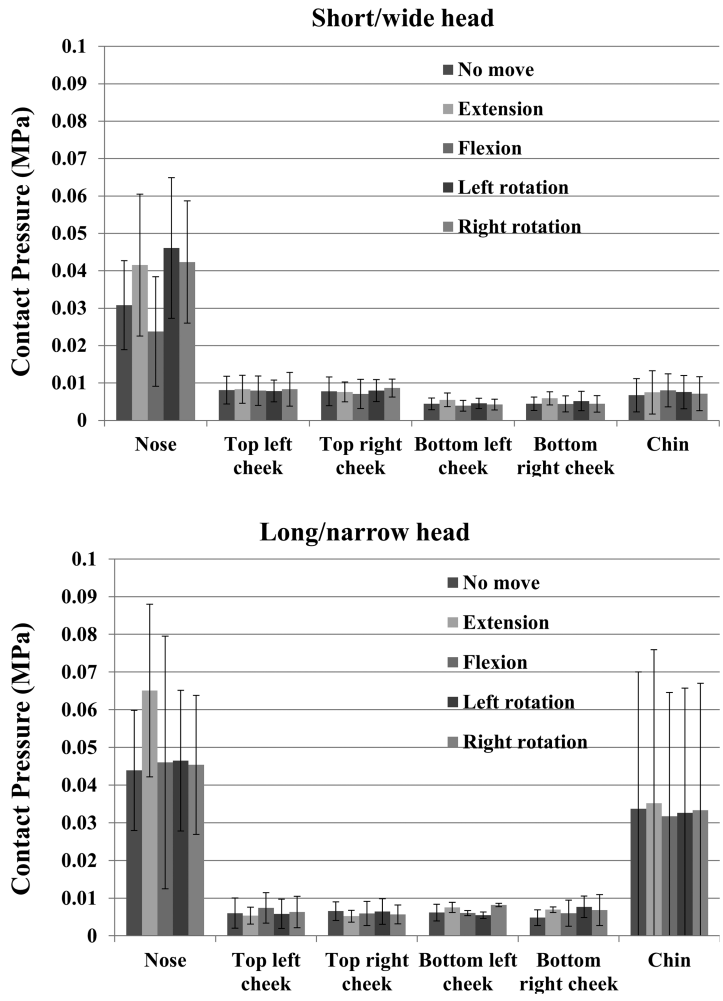

5 *Continued*

the nose ($P < 0.005$), the left rotation significantly changed those at the top of right cheek ($P = 0.03$), and the extension changed those at the bottom of left/right cheek ($P = 0.01$).

Head movements do affect the maximum contact pressures at the nose for all five headforms. For each key area of a headform, the mean maximum contact pressure difference between a head movement case and head fixed case was calculated (Fig. 5). The extension and left/right rotations largely increased the mean maximum contact pressures at the nose for all five headforms (0.008–0.029 MPa) except the left/right rotation for the long/narrow headform. Head flexion largely decreased the mean maximum contact pressures at the nose for the medium and short/wide headforms (−0.011 and −0.007 MPa), and largely increased the ones for the small headform (0.008 MPa). In addition, the left/right rotations largely increased the chin maximum contact pressure for the small headform (0.010 MPa). As presented in Fig. 5, the other pressure changes caused by the head movements were between −0.004 to 0.004 MPa.

From simulation results with the three FFR manufacturers, head movements have a significant effect on the maximum contact pressure at the nose. For each FFR manufacturer, the effects of the head movements on the maximum contact pressure were also investigated by comparing a head movement case with a fixed head case (Fig. 6). The extension and left/right

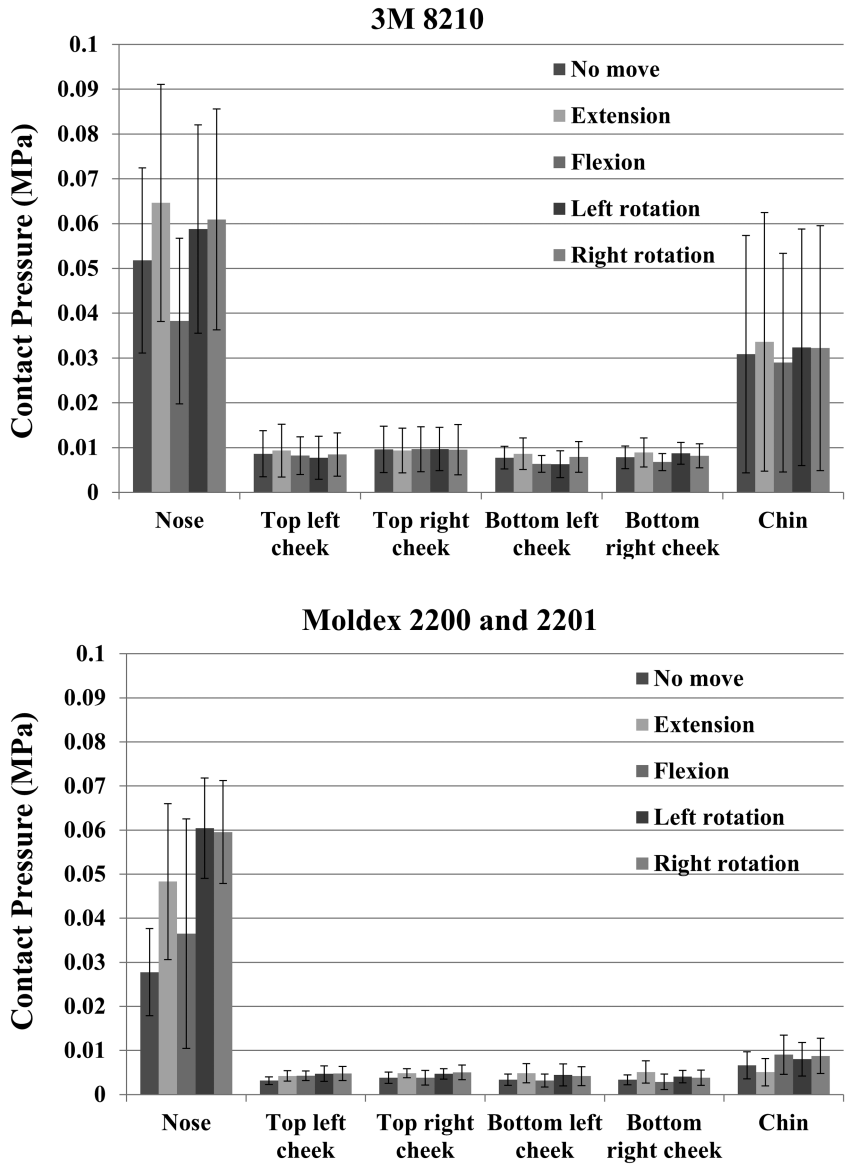

6 Means and standard deviations of maximum contact pressures at six key areas under five head movement cases: (a) 3M 8210; (b) Moldex 2200 and 2201; and (c) Sperian XL, ML, and S.

rotations largely increased the mean maximum contact pressures at the nose for all three FFR manufacturers (0.09–0.033 MPa), except the left/right rotations for Sperian XL, M/L, and S. The flexion largely changed the mean maximum contact pressures at the nose for 3M 8210 and Sperian XL, M/L, and S by −0.013, 0.008, and −0.006 MPa. As presented in Fig. 6, maximum contact pressure changes in other key areas caused by the head movements were below 0.004 MPa.

The left and right rotations caused larger increases (0.033 and 0.032 MPa) of the nose maximum contact pressures for the Moldex 2200 and 2201 than those for other FFR sizing systems (0.007 and 0.009 MPa for 3M 8210, and 0.003 and 0.003 MPa for Sperian XL, M/L, and S) as shown in Fig. 6. Note that the Moldex 2200 and 2201 models did not have separate nasal clips, which the 3M 8210 and the Sperian XL, M/L, and S had. The results indicated that the use of a nose clip

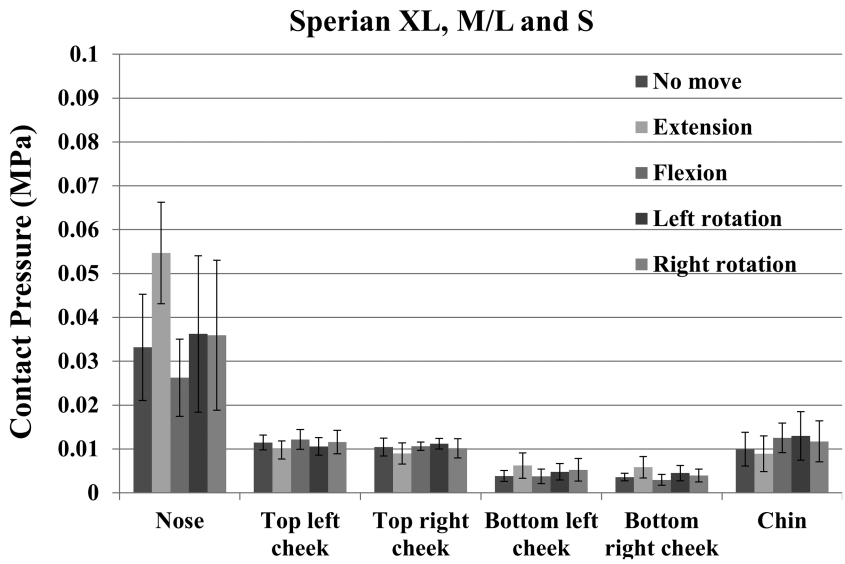

6 *Continued*

could reduce the impact of the left/right rotations on the maximum contact pressure changes at nose area.

The 3M 8210 had higher maximum contact pressures at the bottom cheek and chin (about 0.01 and 0.03 MPa) than other FFR models had (about 0.005 and 0.01 MPa). The contact pressures at the bottom cheek and chin is related the force of the lower FFR strap. The 3M 8210 model's lower strap had higher elastic stiffness than other models' straps had, generating higher forces. The 3M 8210's maximum contact pressures at the chin may cause pressure related discomfort. The small head/Sperian S combination had maximum contact pressures at the bottom cheek below 0.002 MPa, suggesting a loose seal. Thus, the lower straps of the 3M 8210 and Sperian S need to be optimized for respirator fit and comfort.

The sources of the maximum contact pressure changes were the variations of facial deformations and strap tensions during head movements. The strap tensions were related to the strap stiffness and the head size, which were approximately constant. Hence, the strap tension variations had limited influence on the maximum contact pressure changes. The facial deformation variations played an essential role in the maximum contact pressure changes. The flexion and extension changed the chin anterior part soft tissue thickness about 3 and −1.5 mm, and the left/right rotations changed the lateral parts of the chin soft tissue thickness about ±1 mm. The impact of the head movements on the soft tissue thicknesses of other facial areas was not statistically significant.

In all headform/FFR contact simulations, the pressure contours of the key nose area had high contact pressure areas (Figs 2 and 3). It was found that the head movements changed the pressure contours of the key nose area. In the head flexion/extension case the maximum contact pressure location moved up/down about 2 mm along the frontal side of the nasal bridge. In the left/right rotation cases, the maximum contact pressure location moved left/right about 3 mm along the lateral side of the nasal bridge. For other key areas, the change of the contact pressure contours was not statistically significant.

The fit-testing exercises of head side to side and head up and down decrease the protection factor, and do not affect subjects' breathing (Lee *et al.*, 2005; Grinshpun *et al.*, 2009). The faceseal between a headform and a respirator is achieved by the headform and respirator contact. Thus, in experiments it is assumed that the contact change between the respirator and the human face causes protection factor variation during head movements (Crutchfield *et al.*, 1999; Grinshpun *et al.*, 2009; He *et al.*, 2013). However, no known experiments have measured the respirator contact changes with head movements. The simulation results showed that head movements changed the maximum contact

pressures, and in general the distribution of the contact pressure became more uneven in all the key areas studied. This suggests that the likelihood of facial leaks has increased, matching well with the experimental findings. In addition, the simulation-based results found that the nose area was the most sensitive area to head movements. This result also agrees with findings from experiments that during respirator fit test most leaks happened at the nose area and the cheek (Oestenstad et al. 1990; 2010; Roberge *et al.*, 2011). Future work should quantitatively characterize the relationship between the contact pressure changes caused by head movements and respirator fit factors.

Radonovich *et al.* (2009) reported that subjects wearing N95 FFRs experienced facial discomfort or pain due to the contact pressure between the face and respirator. Our simulation results suggest that the maximum contact pressures increase with head movements, especially at the nose area, suggesting that discomfort levels may increase with head movements.

The proposed simulation-based method for headform/FFR contact can be used to assess an FFR design. For example, the contact simulations between 3M 8210 FFR and five headforms were conducted, and the maximum contact pressures at six key areas were obtained. The key areas of the medium and short/wide headforms had smallest variation of the maximum contact pressures, although the medium headform had a high pressure at the nose (0.075 MPa). Hence, the 3M 8210 FFR best fitted the medium and short/wide headforms. The long term goal of this work is to develop a validated simulation tool to assess new respirator in the early design stage to save time.

When a person wears a respirator, there should be a seal check that includes adjusting the strap positions and the nasal clip. Our headform/FFR contact simulations contained the step of deforming the nasal clip for better fitting the nasal bridge. However, the procedure of adjusting the strap positions was not considered here and will be included in the future study.

Note that in this study, we only simulated final positions of head movements instead of the entire dynamic movement period. However, it is technically feasible to simulate the whole process based on the available simulation model depending on the CPU time availability. Therefore, our future work will include the whole dynamics head movement simulation and experimental validation of the contact pressure changes.

SUPPLEMENTARY DATA

Supplementary data can be found at http://annhyg.oxfordjournals.org/.

FUNDING

National Institute for Occupational Safety and Health (NIOSH) projects (Awards # 254-2009-M-31878, 254-2010-M-36735, and 254-2012-M-52258).

ACKNOWLEDGEMENTS

The authors appreciate the anonymous reviewers for the constructive comments and suggestions to improve the quality of this article.

DISCLAIMER

The findings and conclusions in this article are those of the authors and do not necessarily represent the views of the National Institute for Occupational Safety and Health.

REFERENCES

Crutchfield CD, Fairbank EO, Greenstein SL. (1999) Effect of test exercises and mask donning on measured respirator fit. *Appl Occup Environ Hyg*; 14: 827–37.

Grinshpun SA, Haruta H, Eninger RM *et al.* (2009) Performance of an N95 filtering facepiece particulate respirator and a surgical mask during human breathing: two pathways for particle penetration. *J Occup Environ Hyg*; 6: 593–603.

He X, Grinshpun SA, Reponen T *et al.* (2013) Laboratory evaluation of the particle size effect on the performance of an elastomeric half-mask respirator against ultrafine combustion particles. *Ann Occup Hyg*; 57: 884–97.

Lee SA, Grinshpun SA, Adhikari A *et al.* (2005) Laboratory and field evaluation of a new personal sampling system for assessing the protection provided by the N95 filtering facepiece respirators against particles. *Ann Occup Hyg*; 49: 245–57.

Lei Z, Yang J. (2010a) *Toward High Fidelity Respirator and Headform Models*. In 1st International Conference on Applied Digital Human Modeling, July 17–20, Miami, FL.

Lei Z, Yang J, Zhuang Z. (2010b) Contact pressure study of N95 filtering facepiece respirators using finite element method. *Comput Aided Design Appl*; 7: 847–61.

Lei Z, Yang J, Zhuang Z. (2012) Headform and N95 filtering facepiece respirator interaction: contact pressure simulation and validation. *J Occup Environ Hyg*; 9: 46–58.

Lei Z, Yang J, Zhuang Z, Roberge R. (2013) Simulation and evaluation of respirator faceseal leaks using computational fluid dynamics and infrared imaging. *Ann Occup Hyg*; 57: 493–506.

Lei Z, Ji X, Zhuang Z, Rottach D, Yang J. (2014) Simulated effects of head movement on contact pressures between

headforms and N95 filtering facepiece respirators-part 1: headform model and validation. *Ann Occup Hyg*.

Occupational Safety and Health Administration (OSHA) (1999) Respiratory Protection. *OSHA Technical Manual (OTM)*, section VIII: Chapter 2.

Oestenstad RK, Dillion HK, Perkins LL. (1990) Distribution of faceseal leak sites on a half-mask respirator and their association with facial dimensions. *Am Ind Hyg Assoc J*; 51: 285–90.

Oestenstad RK, Bartolucci AA. (2010) Factors affecting the location and shape of face seal leak sites on half-mask respirators. *J Occup Environ Hyg*; 7: 332–41.

Radonovich LJ Jr, Cheng J, Shenal BV *et al.* (2009) Respirator tolerance in health care workers. *JAMA*; 301: 36–8.

Roberge RJ, Monaghan WD, Palmiero AJ *et al.* (2011) Infrared imaging for leak detection of N95 filtering facepiece respirators: a pilot study. *Am J Ind Med*; 54: 628–36.

Schaff AJ, Ogale AA. (1991) Tensile viscoelastic properties of spunbonded nonwoven polypropylene backing. *Textile Res J*; 61: 386–92.

Sun H, Pan N, Postle R. (2005) On the Poisson's ratios of a woven fabric. *Compos Struct*; 68: 505–10.

Zhuang Z, Bradtmiller B, Shaffer RE. (2008) New respirator fit test panels representing the current U.S. Civilian Work Force. *J Occup Environ Hyg*; 4: 647–59.

Zhuang Z, Benson S, Viscusi D. (2010) Digital 3-D headforms with facial features representative of the current US workforce. *Ergonomics*; 53: 661–71.